

# lncRNA DUXAP8 Facilitates Multiple Malignant Phenotypes and Resistance to PARP Inhibitor in HCC via Upregulating FOXM1

Yu Hu,<sup>1</sup> Xian Zhang,<sup>2</sup> Hong-Yan Zai,<sup>1</sup> Wei Jiang,<sup>1</sup> Liang Xiao,<sup>1</sup> and Qin Zhu<sup>1</sup>

<sup>1</sup>Department of General Surgery, Xiangya Hospital, Central South University, Changsha 410008, Hunan Province, P.R. China; <sup>2</sup>Department of Occupational and Environmental Health, Xiangya School of Public Health, Central South University, Changsha 410008, Hunan Province, P.R. China

**In this study, we examined the clinical significance and molecular mechanisms of a long non-coding RNA (lncRNA), double homeobox A pseudogene 8 (DUXAP8) in hepatocellular carcinoma (HCC). DUXAP8 expression was compared using quantitative real-time PCR in HCC versus adjacent tissues and in HCC cell lines versus normal hepatic epithelial cells. The correlations between DUXAP8 level and clinicopathological features were analyzed. Assays including MTT, colony-forming analysis, Transwell assay, western blot, xenograft formation, experimental metastasis, luciferase assay, RNA pull-down, and RNA immunoprecipitation were used to examine DUXAP8-induced malignant phenotypes, its regulation on forkhead box protein M1 (FOXM1), and the importance of FOXM1 in mediating DUXAP8 phenotypes. Our results showed that DUXAP8 was significantly upregulated in HCC tissues or cell lines associated with tumors of advanced grades, tumors that were positive for lymph node metastasis, and patients with poor overall survival. DUXAP8 was essential in maintaining multiple malignant phenotypes (including resistance to olaparib) both *in vitro* and *in vivo*. Mechanistically, DUXAP8 upregulated FOXM1 expression by sponging miR-485-5p and interacting with the RNA-binding protein Fused in Sarcoma (FUS). Functionally, FOXM1 essentially mediated the oncogenic phenotypes of DUXAP8. Collectively, DUXAP8 acts through two distinct mechanisms to upregulate FOXM1 and becomes a pleiotropic oncogenic lncRNA in HCC.**

## INTRODUCTION

Hepatocellular carcinoma (HCC) is the predominant form of primary liver cancer, accounting for 70%–85%.<sup>1</sup> In China, the prevalence of chronic infection of hepatitis B virus and hepatitis C virus significantly contributes to the high morbidity (responsible for >55% of all HCC cases worldwide) and mortality of HCC.<sup>2</sup> Although vaccination and other prevention strategies may lower the incidence and mortality of HCC by more than 40% through 2030 in China, it remains an aggressive malignancy with a median survival between approximately 6 and 20 months.<sup>3</sup> The complex and yet not so well-understood pathogenesis suggest that a multimodality strategy is required for HCC therapy. Therefore, it is critical to identify new diagnostic and/or prognostic biomarkers and to understand molecu-

lar pathogenic mechanisms that may facilitate the development of effective therapeutic strategies.

The defect in the DNA repair system is a significant pathogenic factor in cancer development. Poly(ADP-ribose) polymerase (PARP) is a family of enzymes that catalyze the posttranslational conjugation of poly(ADP-ribose) to target proteins and regulate multiple cellular processes. The best characterized PARP family member, PARP1, plays an essential role in the base excision repair (BER) pathway of repairing DNA single-strand breaks.<sup>4</sup> While the breast cancer gene 1 (BRCA1) and BRCA2 critically regulate the homologous recombination (HR) pathway repairing DNA double-strand breaks,<sup>5</sup> in cells with deficient BRCA1 or BRCA2 functions, BER is the default DNA repair pathway. Therefore, targeting PARP signaling may lead to the death of cancer cells with mutations in BRCA1 and/or BRCA2, a phenomenon known as synthetic lethality.<sup>6</sup> In support of this concept, a few PARP inhibitors (PARPis), including olaparib, rucaparib, and niraparib, have been approved by the Food and Drug Administration (FDA) and the European Medicine Agency for treatment of ovarian or breast cancers, particularly those bearing BRCA mutations (<https://www.fda.gov>). Meanwhile, more PARPis are being tested in pre-clinical and clinical trials. The success of the PARPi in cancer treatment is also accompanied by the increasing realization that many patients do develop resistance through diverse mechanisms.<sup>7,8</sup> For example, Fang et al.<sup>9</sup> recently reported that forkhead box protein M1 (FOXM1), a transcription factor and a master regulator of DNA damage repair, disrupted the sensitivity of cells to PARPis. For HCC, a few clinical trials on PARPis have been performed, and the available results are disappointing,<sup>10</sup> which suggests the presence of mechanisms resistant to PARPis. Identifying these mechanisms will not only help to predict treatment response of HCC patients to PARPi but also promote the development of therapies that confer sensitivity to PARPis.

Received 21 April 2020; accepted 17 October 2020;  
<https://doi.org/10.1016/j.omto.2020.10.010>

**Correspondence:** Qin Zhu, MD, Department of General Surgery, Xiangya Hospital, Central South University, No. 87 Xiangya Road, Changsha 410008, Hunan Province, P.R. China.

**E-mail:** [zhuqinqinn13@163.com](mailto:zhuqinqinn13@163.com)



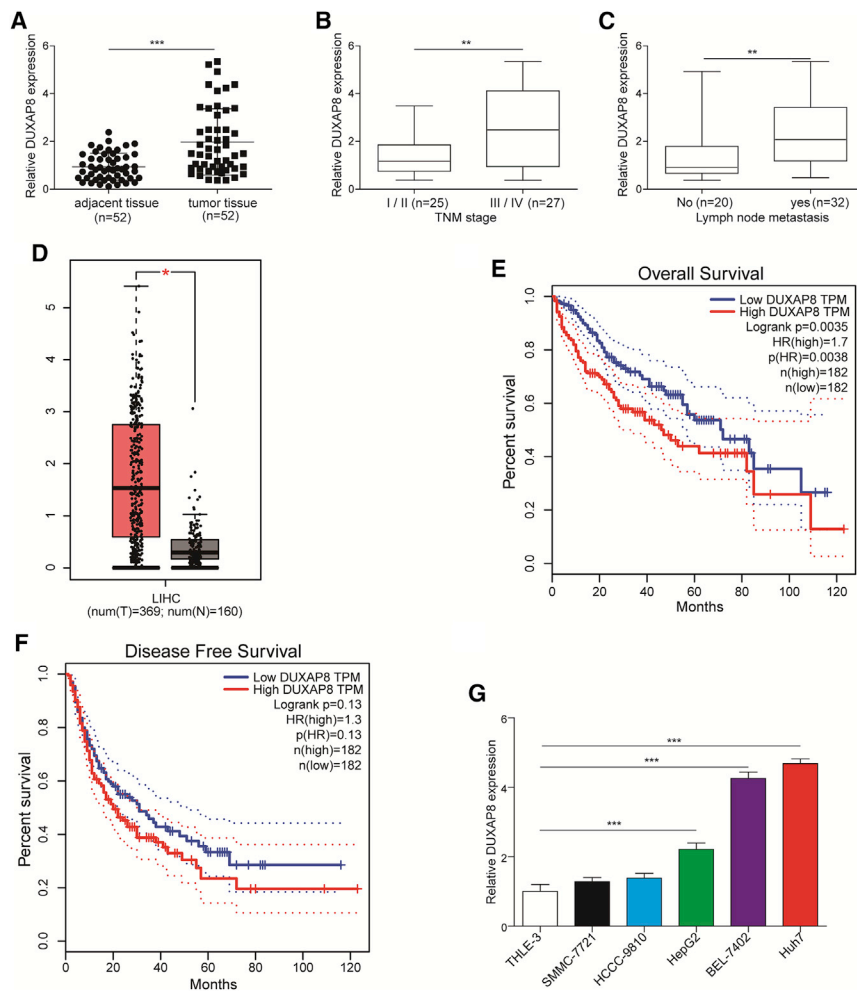


**Figure 1. DUXAP8 Was Upregulated in HCC Tissues and Cell Lines and Associated with Worse Prognosis**

(A–C) The expression of DUXAP8 was examined by quantitative real-time PCR, presented as relative ratio to the level of internal control GAPDH, and compared between 52 pairs of HCC tissues and the matching para-tumor tissues (A), between HCC tumors of TNM stage I/II ( $n = 25$ ) and those of stage III/IV ( $n = 27$ ) (B), and between HCC tumors negative ( $n = 20$ ) and positive ( $n = 32$ ) for lymph node metastasis (C). (D–F) TCGA database analysis through the GEPIA portal compared DUXAP8 expression between HCC ( $n = 369$ ) and normal tissues ( $n = 160$ ) (D) and the association between DUXAP8 expression and overall survival (E) or disease-free survival (F) of HCC patients ( $n = 364$ ). (G) The expression of DUXAP8 was compared between human HCC cell lines HCC9810, BEL-7402, Huh7, SMMC-7721, HepG2, HepG2/ADR, and normal THLE-3 hepatocytes. \* $p < 0.05$ ; \*\* $p < 0.01$ ; \*\*\* $p < 0.001$ .

## RESULTS

### DUXAP8 Was Upregulated in HCC Tissues and Cell Lines and Associated with Worse Prognosis

A recent study identified DUXAP8 as a robustly upregulated lncRNA that associated with poor overall survival of HCC patients.<sup>14</sup> To explore the mechanisms by which DUXAP8 act in HCC, we collected 52 pairs of HCC tissues and matching para-tumor tissues to assess the expression of DUXAP8. As shown in Figure 1A, DUXAP8 was significantly upregulated in cancer tissues compared with para-tumor tissues ( $p < 0.001$ ). Further stratification analyses re-

vealed that DUXAP8 expression was markedly elevated in Tumor Node Metastasis (TNM) stage-III/IV tumors ( $n = 27$ ), compared with that in stage-I/II tumors ( $n = 25$ ;  $p < 0.01$ ; Figure 1B), and also in those positive for lymph node metastasis ( $n = 32$ ) compared with those negative ( $n = 20$ ;  $p < 0.01$ ; Figure 1C). Consistently, The Cancer Genome Atlas (TCGA) database analysis through the Gene Expression Profiling Interactive Analysis (GEPIA) website (<http://gepia.cancer-pku.cn/index.html>) showed that: first, the DUXAP8 level from HCC tissues ( $n = 369$ ) was robustly higher than that from normal tissues ( $n = 160$ ;  $p < 0.05$ ; Figure 1D); second, a higher level of DUXAP8 ( $n = 182$ ) was significantly correlated with worse overall survival ( $p = 0.0035$ ; Figure 1E) of HCC patients; and third, there was no significant correlation between DUXAP8 level and the disease-free survival of HCC patients ( $p = 0.13$ ; Figure 1F). When examining DUXAP8 expression among different HCC cell lines—namely, HCCC-9810, BEL-7402, Huh-7, SMMC-7721, HepG2, and HepG2/ADR—we observed that its level was markedly higher than in normal liver epithelial cell line THLE-3 (all  $p < 0.05$ ; Figure 1G). With all data taken together, DUXAP8 is upregulated in HCC tissues

Mounting evidence suggests that long noncoding RNAs (lncNRAs)—non-protein-coding RNAs with more than 200 nucleotides and capable of interacting with DNA, RNA, and proteins—play diverse roles in cancer progression and function not only as diagnostic biomarkers but also as therapeutic targets.<sup>11–13</sup> Among them, the double homeobox A pseudogene 8 (DUXAP8) is a pseudogene-derived lncRNA upregulated in a variety of human cancers and serves as a pan-cancer diagnostic and/or prognostic biomarker.<sup>14</sup> Earlier studies on HCC showed that DUXAP8 expression increased, was an unfavorable prognostic biomarker, and promoted the proliferation and invasion of tumor cells.<sup>14,15</sup> However, the mechanisms underlying the oncogenic activities of DUXAP8 remain largely unknown. In the present study, we aim to characterize biological effects and molecular mechanisms of DUXAP8 in HCC. Through bioinformatic analysis, we identified that DUXAP8 may interact with miR-485-5p, which may also interact with FOXM1. This clue prompted us to focus on the DUXAP8/miR-485-5p/FOXM1 axis and its importance in HCC development.

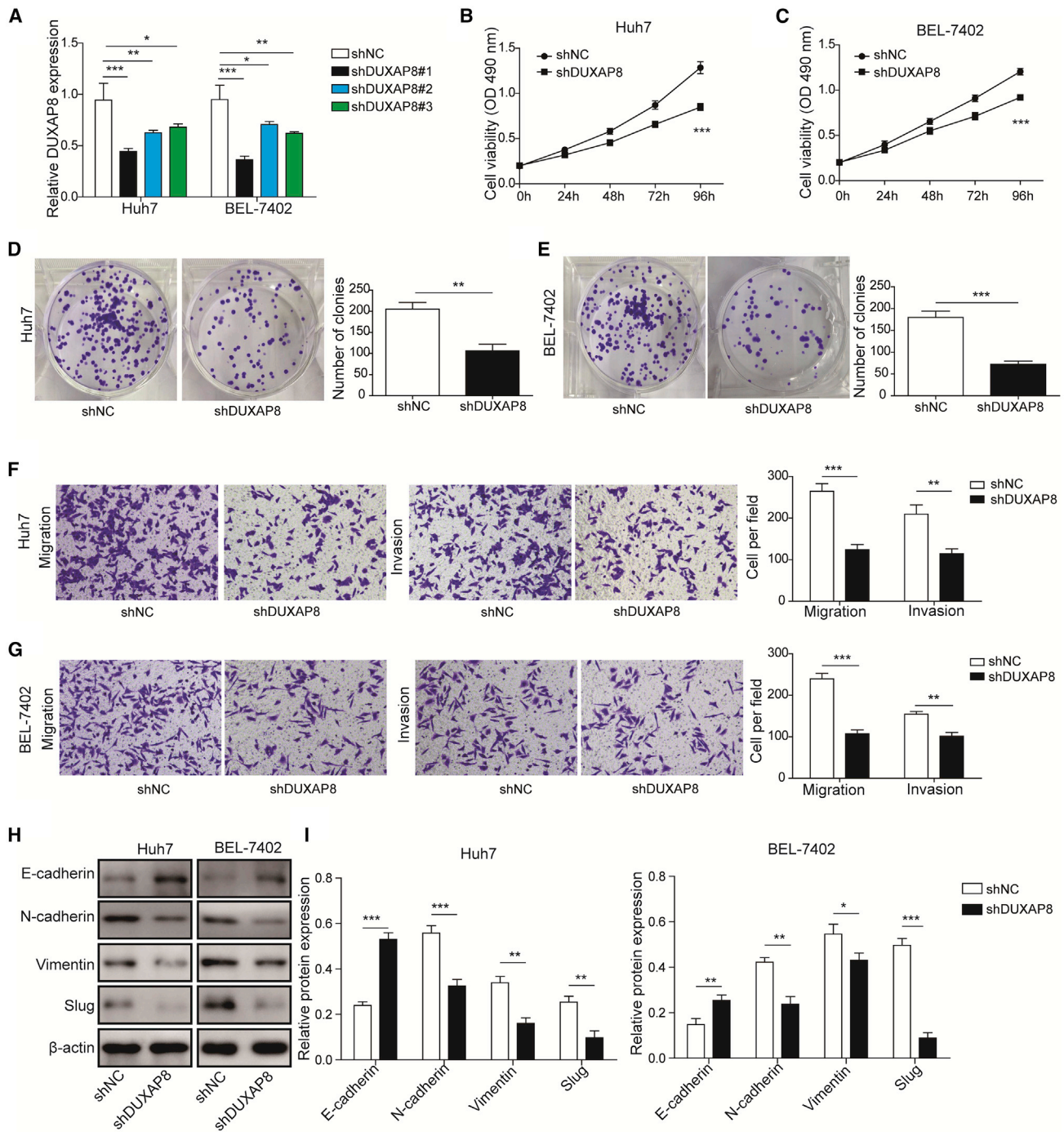


**Figure 2. DUXAP8 Promoted Multiple Malignant Phenotypes of HCC Cells**

(A) Huh7 and BEL-7402 cells were stably transfected with three distinct shDUXAP8 vectors. The expression of DUXAP8 was examined by quantitative real-time PCR and compared to that in cells transfected with shNC. (B and C) The cell viability of shNC versus shDUXAP8 Huh7 (B) and BEL-7402 (C) cells was examined by MTT assay. (D and E) Colony-forming assay was performed to assess the long-term proliferation of shNC versus shDUXAP8 Huh7 (D) and BEL-7402 (E) cells. Representative images of colonies formed are presented on the left, and the quantification of the number of colonies formed is presented on the right. (F and G) The migration and invasion of shNC versus shDUXAP8 Huh7 (F) and BEL-7402 (G) cells were examined by Transwell assays. Representative images of migrated cells

(legend continued on next page)

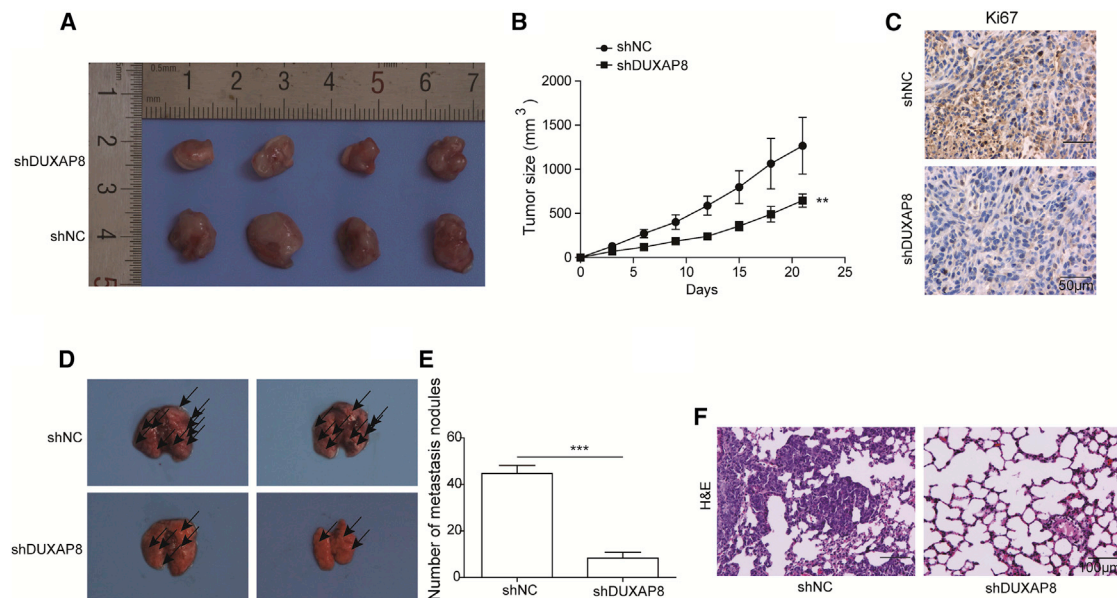


**Figure 3. Targeting DUXAP8 Suppressed *In Vivo* Xenograft Growth and Metastasis**

shDUXAP8 versus shNC BEL-7402 cells were subcutaneously injected into nude mice ( $n = 4$  per group). (A and B) The picture (A) and growth curve (B) of xenografts from all mice in each group. (C) Representative IHC images of Ki-67 staining on the xenografts. shDUXAP8 versus shNC BEL-7402 cells were intravenously injected into nude mice ( $n = 5$  per group). (D) The picture of representative lung tissues from each group. (E) Quantification of metastasis nodules within the lung tissues of each group. (F) Representative H&E staining images of the lung tissues from each group. \*\* $p < 0.01$ ; \*\*\* $p < 0.001$ .

and cell lines, and its elevated expression correlates with tumors of higher malignancy or patients with worse prognosis, supporting that DUXAP8 is an oncogenic lncRNA in HCC.

#### DUXAP8 Promoted Multiple Malignant Phenotypes of HCC Cells

To understand the molecular mechanisms underlying the action of DUXAP8 in HCC, we chose BEL-7402 and Huh-7 cells as the model system, which represents HCC cells expressing high levels of endogenous DUXAP8, and adopted the loss-of-function strategy by stably expressing three different short hairpin RNA (shRNA) sequences specifically targeting DUXAP8 (shDUXAP8)—#1, #2, and #3—in these cells. As shown in Figure 2A, shDUXAP8#1 demonstrated the most robust effect in knocking down DUXAP8 in both cells (both  $p$ s  $< 0.001$ , when compared to shNC [negative control]-expressing cells) and thus was used for subsequent experiments, where it was referred to as shDUXAP8. Corresponding to the reduction of DUXAP8, when compared to the corresponding shNC cells, shDUXAP8 cells presented significantly reduced viability (as determined by 3-(4, 5-dimethylthiazolyl)-2, 5-diphenyltetrazolium bromide [MTT] assay; both  $p$ s  $< 0.001$  [Figures 2B and 2C]), colony formation (as shown by colony-forming assay;  $p < 0.01$  for Huh7 [Figure 2D] and  $p < 0.001$  for BEL-7402 cells [Figure 2E]), migration and invasion (as measured using Transwell migration/invasion assay;  $p < 0.001$  for migration and

$p < 0.01$  for invasion [Figures 2F and 2G]), and epithelial-to-mesenchymal transition ([EMT] as represented by increased expression of epithelial biomarker E-cadherin and reduced expressions of mesenchymal biomarkers, N-cadherin, vimentin, and slug; all  $p < 0.05$  [Figures 2H and 2I]), supporting that DUXAP8 plays an essential role in maintaining multiple malignant phenotypes of HCC cells.

#### DUXAP8 Stimulated Xenograft Growth and Experimental Metastasis of HCC Cells

In addition to examining the effects of DUXAP8 on HCC cells cultured *in vitro*, we established xenograft models using shDUXAP8 or shNC BEL-7402 cells and monitored the *in vivo* xenograft growth. Consistent with the viability-suppressing effect of shDUXAP8 *in vitro*, shDUXAP8 BEL-7402 cells generated smaller xenografts (Figure 3A) that resulted from significantly thwarted *in vivo* growth ( $p < 0.01$ , when compared to xenografts derived from shNC cells; Figure 3B). Consistently, staining for Ki67, a biomarker for proliferating cells, showed that the proliferating activity was markedly lower in shDUXAP8 xenografts than in shNC ones (Figure 3C). Furthermore, we compared the experimental lung metastasis of shDUXAP8 and shNC HCC cells. Figure 3D showed that knocking down DUXAP8 in BEL-7402 cells potentially reduced the metastatic capacity of these cells. The difference in the number of metastatic nodules was

(left two panels) and invaded cells (middle two panels), as well as the quantification of the number of migrated or invaded cells per field (right panel) are shown. (H) The expressions of EMT-related biomarkers, including E-cadherin, N-cadherin, Vimentin, and Slug, in shNC versus shDUXAP8 Huh7 and BEL-7402 cells were examined by western blot. GAPDH was examined as the internal control. (I) The relative expressions of indicated genes were quantified from western blot. \* $p < 0.05$ ; \*\* $p < 0.01$ ; \*\*\* $p < 0.001$ .

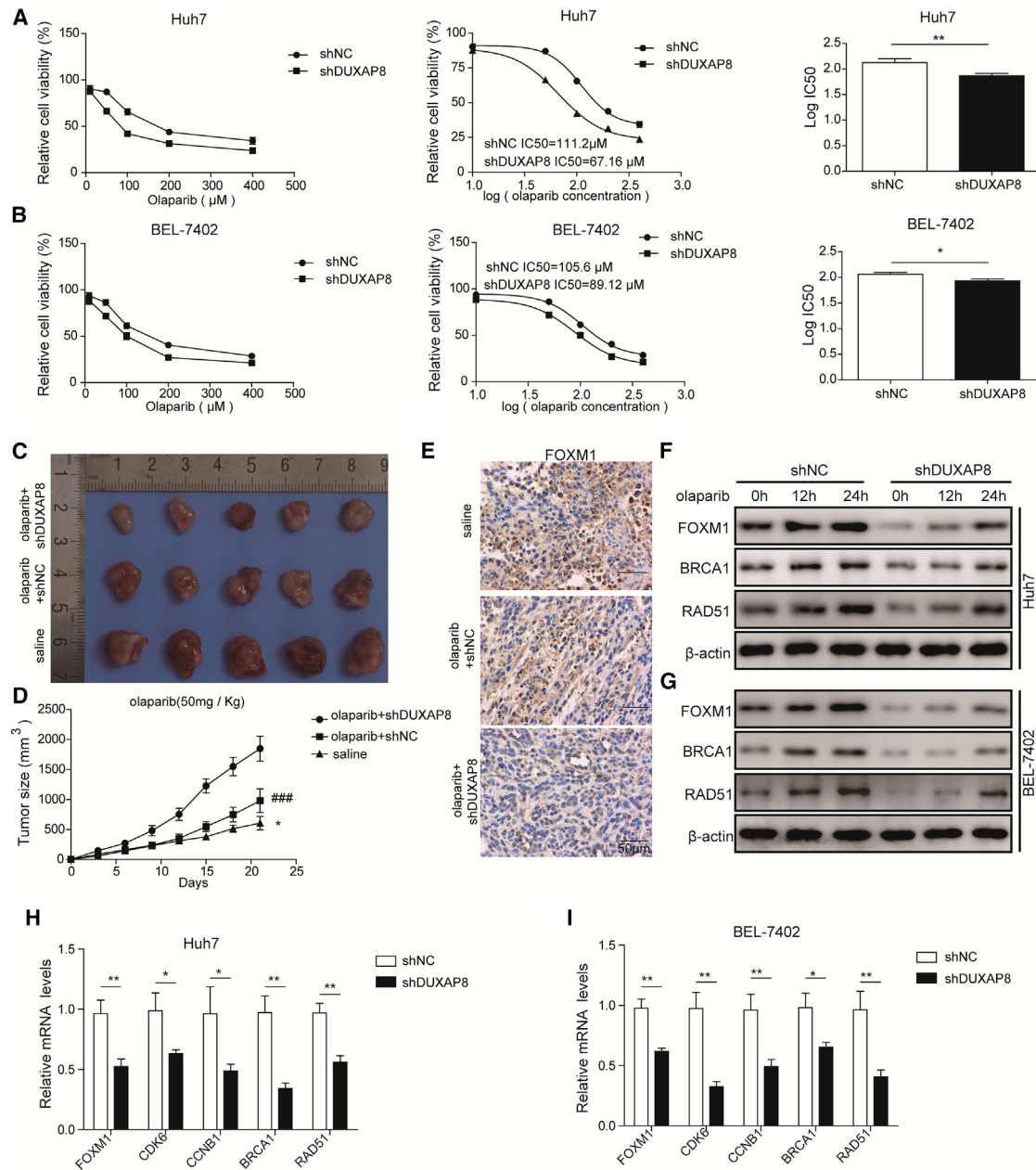


**Figure 4. Knocking Down DUXAP8 Enhanced the Sensitivity of HCC Cells to PARPis**

(A and B) shDUXAP8 versus shNC Huh7 (A) and BEL-7402 (B) cells were treated with olaparib at indicated concentrations for 48 h. Cell viability was examined by MTT assay (left two panels), and  $\log_{10} \text{IC}_{50}$  was calculated (right panel). shDUXAP8 versus shNC BEL-7402 cells were subcutaneously injected into nude mice ( $n = \text{per group}$ ), and mice were treated with either olaparib or saline. (C and D) The picture (C) and growth curve (D) of xenografts from all mice in each group. (E) Representative IHC images of FOXM1 staining on the xenografts. shDUXAP8 versus shNC Huh7 and BEL-7402 cells were treated with olaparib for 0, 12, and 24 h, respectively. (F and G) The expressions of FOXM1, BRCA1, RAD51, and  $\beta$ -actin (internal control) were examined by western blot for Huh7 cells (F) and BEL-7402 cells (G). (H and I) shDUXAP8 versus shNC HCC Huh7 (H) and BEL-7402 (I) cells were treated with olaparib. The expressions of indicated target genes were examined by quantitative real-time PCR. \* $p < 0.05$ ; \*\* $p < 0.01$ ; \*\*\* $p < 0.001$ .

statistically significant ( $p < 0.001$ , when compared to shNC-expressing cells; Figure 3E) and evident from hematoxylin and eosin (H&E)-stained lung tissues. These data evidence the *in vivo* significance of DUXAP8 in promoting cancer progression and metastasis.

#### Knocking Down DUXAP8 Enhanced the Sensitivity of HCC Cells to PARPis

PARPis presented promising, yet not ideal, therapeutic benefits for HCC.<sup>10,16</sup> To assess whether DUXAP8 impacts the sensitivity of

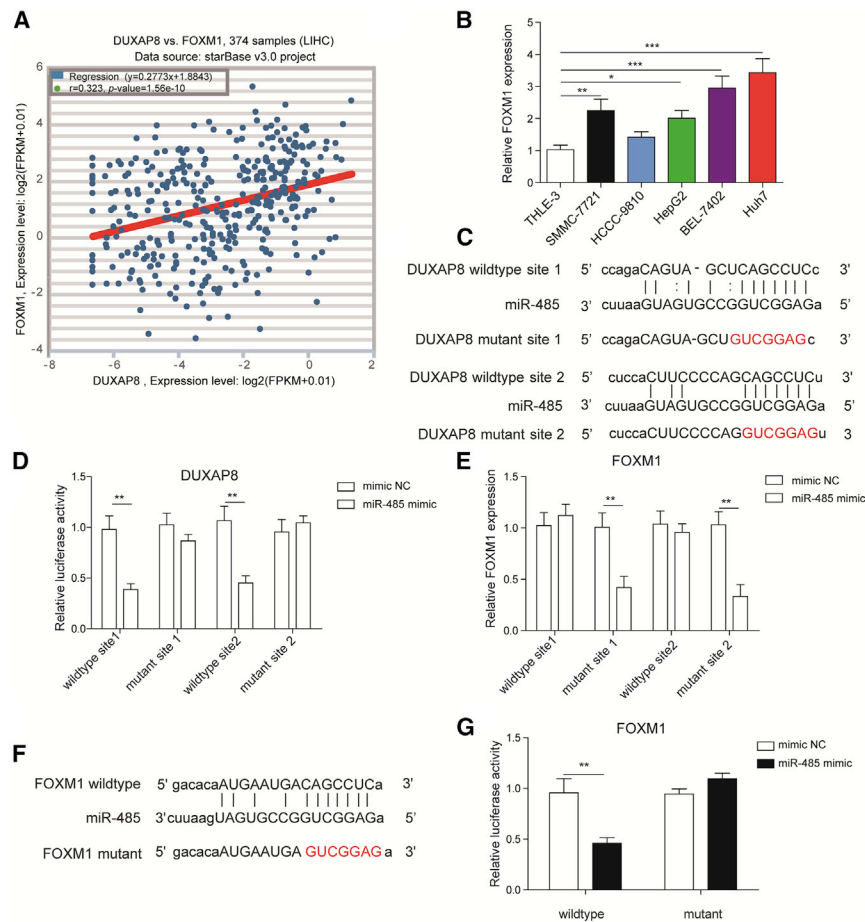


**Figure 5. DUXAP8 Sponged miR-485-5p and Released the Suppression of the Latter on FOXM1**

(A) The correlation between DUXAP8 and FOXM1 expression in HCC tissues ( $n = 374$ ) was examined in TCGA database. (B) The expression of FOXM1 was compared between human HCC cell lines HCC9810, BEL-7402, Huh7, SMMC-7721, HepG2, and normal THLE-3 hepatocytes. (C) Bioinformatic analysis revealed two potential binding sequences within DUXAP8 to miR-485-5p. Mutations were made in both sequences of DUXAP8 gene to disrupt the interaction to miR-485-5p. (D) BEL-7402 cells were transfected with luciferase reporter gene driven by wild-type, mutant site 1, mutant site 2, or mutant site 1/2 (both sequences mutated). The luciferase activity was measured and compared between cells treated with mimic NC and miR-485-5p mimic. (E) The expression of FOXM1 was examined by quantitative real-time PCR in BEL-7402 cells treated as in (D). (F) Bioinformatic analysis revealed one potential binding site within the FOXM1 3' UTR to miR-485-5p. Mutations were made in the binding sequence of FOXM1 to disrupt the interaction to miR-485-5p. (G) BEL-7402 cells were transfected with luciferase reporter gene driven by WT or MUT FOXM1 binding sequence. The luciferase activity was measured and compared between cells treated with mimic NC and miR-485-5p mimic. \*\* $p < 0.01$ ; \*\*\* $p < 0.001$ .

HCC cells to PARPis, we compared the half maximal inhibitory concentration ( $IC_{50}$ ) of olaparib, a PARPi approved by the FDA for cancer treatment, between shDUXAP8 and shNC (both Huh7 and BEL-7402 cells). By measuring the viability of HCC cells in response to different doses of olaparib, we calculated that the  $IC_{50}$  for shDUXAP8 Huh7 cells was  $78.25 \mu\text{M}$ , significantly lower than that for shNC Huh7 cells ( $IC_{50} = 187.33 \mu\text{M}$ ;  $p < 0.01$ ; Figure 4A). Similarly, the  $IC_{50}$  for shDUXAP8 BEL-7402 cells was  $101.39 \mu\text{M}$ , also significantly lower than that for shNC BEL-7402 cells ( $IC_{50} = 157.69 \mu\text{M}$ ;  $p < 0.01$ ; Figure 4B). Consistently, the strongest *in vivo* inhibitory effect on xenograft growth was observed when olaparib was used on shDUXAP8 xenografts (olaparib+shDUXAP8), followed by when olaparib was used on shNC xenografts (olaparib+shNC), as reflected by both the sizes of xenografts isolated on day 21 after the initial inoculation of different BEL-7402 cells (Figure 4C) and by the growth curve of xenografts ( $p < 0.001$  and  $p < 0.01$ , when comparing the saline and olaparib +shDUXAP8 group with the olaparib +shNC group, respectively; Figure 4D). Further immunohistochemistry analysis on the xenografts showed that the expression of FOXM1 was most robustly reduced in the olaparib+shDUXAP8 xenografts (Figure 4E). *In vitro*, olaparib treatment induced, in a time-depen-

dent manner, the expressions of DNA damage repair genes, including *FOXM1*, *BRCA1*, and *RAD51*, on both the protein (Figures 4F and 4G) and mRNA (Figures 4H and 4I) levels. Knocking down DUXAP8 was sufficient to suppress olaparib-induced upregulation of these genes (Figures 4F–4I). Similar effects were also observed on genes regulating cell cycle, including *CDK6* and *CCNB1* (Figures 4H and 4I), suggesting that DUXAP8 essentially controls the sensitivity of HCC cells to PARPis, which may work through its regulation on the expressions of multiple DNA repair and cell-cycle genes.

#### DUXAP8 Sponged miR-485-5p and Released the Suppression of the Latter on FOXM1

Since FOXM1 is an upstream regulator for other DNA repair genes, including *BRCA1* and *RAD51*,<sup>9</sup> we specifically focused on the relationship and regulation between DUXAP8 and FOXM1. Analysis of 374 HCC samples from TCGA database showed that the DUXAP8 level was positively correlated with that of FOXM1 ( $p < 0.001$ ; Figure 5A). Quantitative real-time PCR analysis showed that FOXM1 was significantly upregulated in SMMC-7721, HepG2, BEL-7402, and Huh-7 cells, but not in HCC9810 cells, when compared to normal THLE-3 cells (Figure 5B). Bioinformatic analysis showed that both DUXAP8 and FOXM1 may bind to miR-485-5p, where DUXAP8 contains two potential miR-485-5p-binding sequences (Figure 5C) and FOXM1 contains only one (Figure 5F). Luciferase analysis showed that miR-485-5p

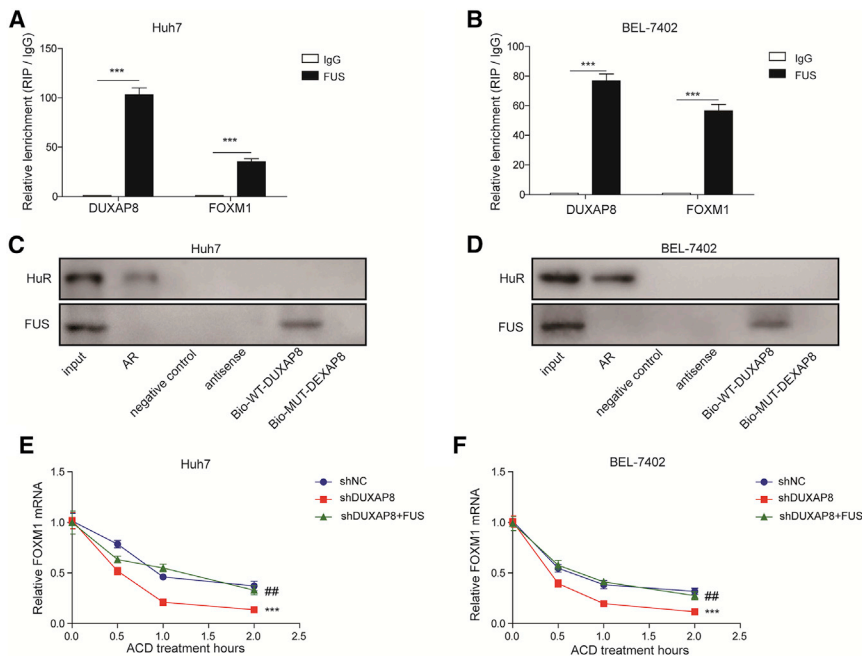


**Figure 6. DUXAP8 Stabilized FOXM1 mRNA by Binding to FUS**

RIP assay revealed the complex formation among DUXAP8, FUS, and FOXM1 mRNA. (A and B) Cellular lysates of Huh7 (A) and BEL-7402 (B) cells were immunoprecipitated using FUS antibody or IgG. DUXAP8 and FOXM1 mRNA levels were determined using quantitative real-time PCR. (C and D) RNA pull-down assay revealed the direct interaction between DUXAP8 and FUS in Huh7 (C) and BEL-7402 (D) cells. Cellular lysates were pulled down using biotinylated WT DUXAP8 probe (Bio-WT-DUXAP8) or DUXAP8 probe containing mutations in the FUS-binding site (Bio-MUT-DUXAP8), and the level of FUS in precipitated samples was determined by western blot. (E and F) shDUXAP8 Huh7 (E) and BEL-7402 (F) cells were transfected with FUS (shDUXAP8+FUS) and treated with actinomycin D to block endogenous transcription. FOXM1 mRNA was then examined at indicated time points by quantitative real-time PCR. \*\*\* $p < 0.001$ .

mimic specifically inhibited the luciferase activity driven by the wild-type (WT) 1 and WT 2 sequences of DUXAP8 ( $p < 0.01$ , when compared to cells treated with mimic NC), and the inhibition was compromised when either or both sites were mutated (MUT) (Figure 5D). Correspondingly, we detected the failure of miR-485-5p mimic to inhibit the endogenous FOXM1 mRNA level in BEL-7402 cells transfected with the luciferase reporter construct containing the WT binding sequence, yet FOXM1 mRNA was significantly reduced in cells co-transfected with miR-485-5p mimic and the luciferase reporter construct containing mutant sequence for site 1, 2, or 1/2 (Figure 5E). Similarly, for the MUT FOXM1 binding sequence, the luciferase activity was no longer affected by miR-485-5p mimic (Figure 5G), suggesting that DUXAP8 sponges miR-485-5p and releases the suppression of the latter on FOXM1.

#### DUXAP8 Stabilized FOXM1 mRNA by Binding to Fused in Sarcoma (FUS)

In addition to sponging microRNA (miRNA), we also examined the potential involvement of FUS, an mRNA stabilizer, in upregulating FOXM1 by DUXAP8. An RNA immunoprecipitation (RIP) assay showed that, in both Huh7 and BEL-7402 cells, FUS bound to both DUXAP8 and FOXM1 mRNA ( $p < 0.001$ , when compared to immunoglobulin G [IgG]; Figures 6A and 6B). The interaction between DUXAP8 and FOXM1 was further confirmed using an RNA pull-down assay (Figures 6C and 6D). To test whether DUXAP8, by acting through FUS, stabilizes FOXM1 mRNA, we measured the decay of FOXM1 mRNA in shNC versus shDUXAP8 Huh7 and BEL-7402 cells in the absence or presence of FUS overexpression. As shown in Figures 6E and 6F, knocking down DUXAP8 (shDUXAP8) specifically accelerated the decay of

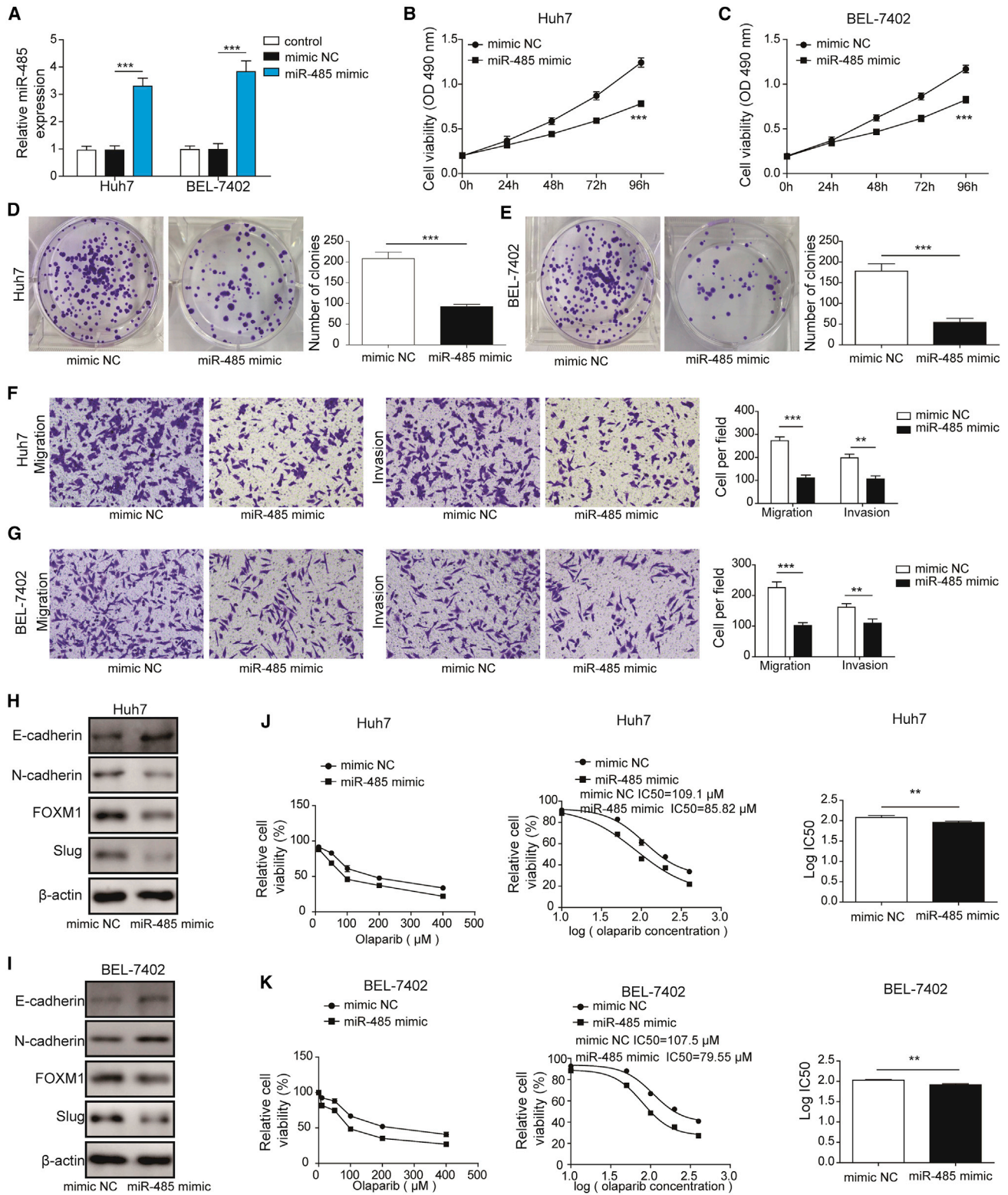
FOXM1 mRNA in both cells ( $p < 0.001$ , when compared to shNC cells), whereas overexpressing FUS in shDUXAP8 cells (shDUXAP8 + FUS) rescued the decay-stimulating effect of shDUXAP8 ( $p < 0.01$ ; comparing shDUXAP8 with shDUXAP8+FUS cells).

#### miR-485-5p Inhibited Multiple Malignant Phenotypes and PARP1 Resistance of HCC Cells

Since DUXAP8 plays an essential role in maintaining multiple malignant phenotypes as well as the sensitivity of HCC cells to the PARPi olaparib, and since we showed earlier that DUXAP8 sponges miR-485-5p and thus upregulates FOXM1, it is therefore interesting to assess the role of miR-485-5p in regulating the malignancy of HCC. For this purpose, we transfected both Huh7 and BEL-7402 cells with miR-485-5p mimic, which significantly boosted the miR-485-5p level, when compared to non-transfected (control) or control-mimic (mimic-NC)-transfected cells ( $p < 0.001$ ; Figure 7A). In response to the elevated level of miR-485-5p, we noticed that the viability (Figures 7B and 7C), long-term proliferation (Figures 7D and 7E), migration/invasion (Figures 7F and 7G), FOXM1 expression, and EMT (Figures 7H and 7I) were all significantly and potently inhibited, whereas the sensitivity to olaparib was significantly enhanced ( $IC_{50}$  was reduced from 200.41  $\mu$ M in mimic-NC-treated Huh7 cells to 130.01  $\mu$ M in miR-485-5p mimic-treated Huh7 cells and from 206.31  $\mu$ M in mimic NC-treated BEL-7402 cells to 105.12  $\mu$ M in miR-485-5p mimic-treated BEL-7402 cells; Figures 7J and 7K), suggesting that miR-485-5p is a tumor-suppressive miRNA that inhibits multiple malignant phenotypes of HCC cells.

#### FOXM1 Essentially Mediated the Oncogenic Activities of DUXAP8

Next, we examined the significance of FOXM1 on the oncogenic activities of DUXAP8 by overexpressing FOXM1 in shDUXAP8 Huh7



(legend on next page)

and BEL-7402 cells (shDUXAP8+FOXM1). Consistent with earlier findings, the expression of FOXM1 was significantly reduced in shDUXAP8 cells alone (shDUXAP8+vector) ( $p < 0.05$ , when compared to the NC cells [shNC+vector]) but was resumed in shDUXAP8+FOXM1 cells (Figure 8A). Correspondingly, the shDUXAP8-induced reductions of cell viability (Figures 8B and 8C) and migration/invasion (Figures 8D and 8E), or increased sensitivity to olaparib (Figures 8F and 8G) (all  $p < 0.01$ , when compared to shNC+vector cells), were all reversed by overexpressing FOXM1 in these cells. Combined with the earlier finding that DUXAP1 upregulated the expression of FOXM1, these data suggest that FOXM1 plays a critical role in mediating the oncogenic activities of DUXAP8.

## DISCUSSION

Pseudogenes are generated when natural mutations accumulate on a protein-coding gene, leading to the decay or degeneration of the transcript.<sup>17</sup> The sequence similarity between pseudogenes and the corresponding protein-coding genes confers the potential for the former to regulate cellular processes in a sequence-specific pattern.<sup>18</sup> Mounting evidence suggests not only that most pseudogenes are actively transcribed, but also that lncRNAs transcribed from pseudogene loci may modulate gene transcription and epigenetic state and function as guides, tethering molecules, or competitive endogenous RNAs (ceRNAs) to sponge miRNAs.<sup>19</sup> In this study, we focused on the pseudogene-derived lncRNA DUXAP8 and presented substantial evidence that DUXAP8 is an oncogenic lncRNA during HCC development: it was essential for maintaining a repertoire of malignant phenotypes of *in vitro* cultured HCC cells, including cell viability, long-term proliferation, migration/invasion, and EMT; knocking down DUXAP8 suppressed the xenograft growth and HCC metastasis *in vivo*; from the clinical perspective, DUXAP8 expression was upregulated in HCC tissues; and its level correlated with that of tumors of higher TNM stages, with positive lymph node metastasis, and with patients with worse overall survival. Consistent with our findings, Jiang et al.<sup>15</sup> reported that upregulated DUXAP8 was significantly associated with the poor outcomes of HCC patients and that downregulating DUXAP8 in HCC cells was sufficient to reduce the viability and colony formation of the cells. Yue et al.<sup>14</sup> showed that DUXAP8 was a potential pan-cancer diagnostic and prognostic biomarker that impacted cell viability, colony formation, and cell migration. The present study provides a more comprehensive analysis on the *in vitro* phenotypes of HCCs, which were corroborated by *in vivo* xenograft formation and metastasis assays. Furthermore,

this study reported for the first time that DUXAP8 mediated the resistance of HCC cells to PARPis and revealed a responsible mechanism, that is, by upregulating FOXM1, either through the sponging of miR-485-5p or through the interaction with FUS. These novel mechanisms provide an explanation for the positive correlation between DUXAP8 and FOXM1 identified in clinical HCC tissues and suggest that both molecules may serve as potential targets for HCC treatment.

Mechanisms underlying the oncogenic activities of DUXAP8 are continuously revealed in different cancer types. In pancreatic cancer, DUXAP8 epigenetically silenced the transcription of tumor suppressors, CDKN1A and KLF2, by recruiting EZH2 and LSD1 to the promoter and inducing histone 3 lysine 27 trimethylation and/or histone 3 lysine 4 dimethylation of target promoters.<sup>20–23</sup> Besides epigenetic regulation, DUXAP8 was also reported to serve as a ceRNA for miR-577 in colorectal cancer and for miR-126 in renal cell carcinoma to promote malignant behaviors of cancer cells.<sup>24,25</sup> By far, epigenetic regulation and sponging miRNAs are the two main mechanisms by which DUXAP8 achieved its oncogenic activities. Our findings from this study showed that DUXAP8 upregulated FOXM1 through two mechanisms, by sponging miR-485-5p and by FUS-mediated mRNA stabilization. Bioinformatic analysis provides important clues suggestive of the DUXAP8/miR-485-5p/FOXM1 axis.

Previous studies also reported the tumor-suppressive activities of miR-485-5p in human cancers, including gastric cancer,<sup>26,27</sup> NSCLC,<sup>28</sup> breast cancer,<sup>29,30</sup> and thyroid cancer,<sup>31,32</sup> and in HCC.<sup>33–36</sup> In HCC, distinct lncRNAs all sponge miR-485-5p and upregulate different downstream targets to accomplish their oncogenic activities.<sup>33,35,36</sup> These studies, when combined with the present one, support the significance of miR-485-5p as a signaling hub linking myriad lncRNAs with downstream targets to deliver malignant phenotypes. Consistently, when it was overexpressed in two different HCC cell lines, we showed that miR-485-5p significantly suppressed multiple malignant phenotypes. It would be interesting for future studies to comprehensively analyze the signaling wheel that hubs miR-485-5p and assess the therapeutic potential/safety of boosting its expression in cancer.

FUS is an RNA-binding protein that regulates pre-mRNA splicing and mRNA transport, stability, and translation.<sup>37</sup> The dreamBase analysis suggests that FUS protein contains interaction sites for 5,106 distinct pseudogenes,<sup>38</sup> yet the specific interaction between FUS and DUXAP8

### Figure 7. miR-485-5p Inhibited Multiple Malignant Phenotypes of HCC Cells

(A) Huh7 and BEL-7402 cells were non-transfected (control) or transfected with mimic NC versus miR-485-5p mimic. (B and C) The cell viability of mimic NC versus miR-485-5p mimic Huh7 (B) and BEL-7402 (C) cells was examined by MTT assay. (D and E) Colony-forming assay was performed to assess the long-term proliferation of mimic NC versus miR-485-5p mimic Huh7 (D) and BEL-7402 (E) cells. Representative images of colonies formed are presented on the left, and the quantification of the number of colonies formed is presented on the right. (F and G) The migration and invasion of mimic NC versus miR-485-5p mimic Huh7 (F) and BEL-7402 (G) cells were examined by Transwell assays. Representative images of migrated cells (left two panels) and invaded cells (middle two panels), as well as the quantification of the number of migrated or invaded cells per field (right panel) are shown. (H and I) The expressions of FOXM1 and EMT-related biomarkers, including E-cadherin, N-cadherin, and Slug in mimic NC versus miR-485-5p mimic Huh7 (H) and BEL-7402 (I) cells were examined by western blot. GAPDH was examined as the internal control. (J and K) Mimic NC versus miR-485-5p mimic Huh7 (J) and BEL-7402 (K) cells were treated with olaparib at indicated concentrations. Cell viability was examined by MTT assay (left two panels), and  $\log(C_{50})$  was calculated (right panel). \*\* $p < 0.01$ ; \*\*\* $p < 0.001$ .

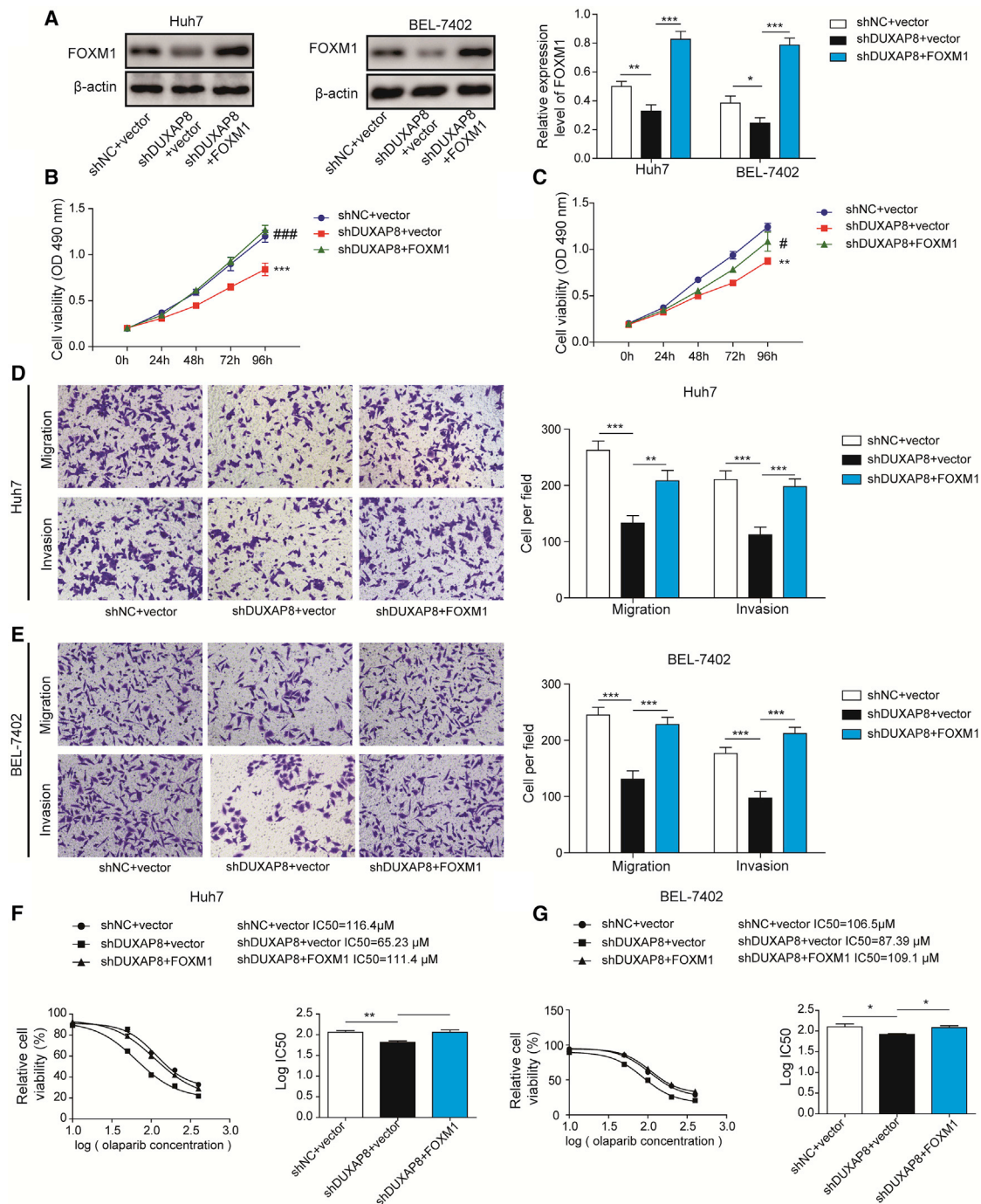


**Figure 8. FOXM1 Mediated the Oncogenic Activities of DUXAP8**

shNC versus shDUXAP8 Huh7 and BEL-7402 cells were transiently transfected with FOXM1-expressing vector or empty vector (NC). (A) The expression level of FOXM1 was detected by western blot with representative image shown on the left and the quantification on the right.  $\beta$ -actin was detected as the loading control. (B and C) The cell viability of indicated Huh7 (B) and BEL-7402 (C) cells was examined by MTT assay. (D and E) The migration and invasion of indicated Huh7 (D) and BEL-7402 (E) cells were examined by Transwell assays. Representative images of migrated cells (left upper panels) and invaded cells (left lower panels), as well as the quantification of the number of migrated or invaded cells per field (right panel) are shown. (F and G) Indicated Huh7 (F) and BEL-7402 (G) cells were treated with olaparib at different concentrations. The logIC<sub>50</sub> was calculated. \*p < 0.05; \*\*p < 0.01; \*\*\*p < 0.001.

**Table 1. Clinical Pathological Characteristics of 52 HCC Patients**

Clinicopathologic Parameter	Number
<b>Gender</b>	
Male	30
Female	22
<b>Age (Years)</b>	
≤60	35
>60	17
<b>Hbsag</b>	
Negative	24
Positive	28
<b>Cirrhosis</b>	
Absence	17
Presence	35
<b>AFP</b>	
≤20	21
>20	31
<b>TNM Stage</b>	
T1/T2	25
T3/T4	27
<b>Microvascular Invasion</b>	
Absence	16
Presence	36
<b>Macrovascular Invasion</b>	
Absence	20
Presence	32
<b>Encapsulation</b>	
Absence	19
Presence	33

or the biological significance of this crosstalk has not been reported before. Here, using RIP and RNA pull-down assays, we showed for the first time that these two molecules interacted. Functionally, knocking down DUXAP8 promoted the decay of FOXM1 mRNA, which was stabilized by overexpressing FUS, supporting the oncogenic activities of FUS. The functional significance of FUS in HCC, however, is under debate, with some studies supporting the anti-cancer activities<sup>39,40</sup> while the others report pro-tumor activities.<sup>41,42</sup> Guo et al.<sup>41</sup> reported that lncRNA SNHG6 was an oncogene for HCC and that one mechanism underlying the oncogenic activities of SNHG6 was by sponging miR-1297 and releasing its inhibition on FUS, the latter impeding the export of MAT1A mRNA from nucleus, downregulating MAT1A protein synthesis, and contributing to genome-wide hypomethylation. In addition, analysis of the HCC gene expression profile GEO: GSE49515 identified FUS as a hub gene whose expression correlated with worse overall survival of HCC patients,<sup>42</sup> which is also consistent with our findings from TCGA database analysis, which re-

vealed that FUS was upregulated in HCC. Therefore, future studies should focus on characterizing the functional roles of FUS in HCC, either as an oncogene or as a tumor suppressor, and understand the molecular mechanisms mediating such functional roles.

FOXM1 is a transcription factor presenting pleiotropic oncogenic activities in human cancers, ranging from proliferation/apoptosis to migration, to EMT, angiogenesis, metastasis, and drug resistance.<sup>43,44</sup> The expression level of FOXM1 in cancer is regulated on multiple levels, including the transcriptional regulation by distinct transcription factors; post-transcriptional regulation by miRNAs; and post-translational modifications such as phosphorylation, acetylation, methylation, ubiquitination, and sumoylation.<sup>44</sup> In this study, we revealed a novel signaling cascade controlling FOXM1 expression in HCC, the DUXAP8/miR-485-5p/FOXM1 axis. We also showed that DUXAP8 may interact with FUS to stabilize FOXM1 mRNA. Functionally, the upregulated FOXM1 was a critical driver in mediating the oncogenic potential of DUXAP8 and was sufficient to induce the proliferation and the migration of HCC cells, as well as their resistance to PARPis. In support of our findings, Fang et al.<sup>9</sup> reported that olaparib induced the expression and nuclear localization of FOXM1, which, in turn, upregulated other HR repair genes such as BRCA1 and RAD51, and contributed to olaparib-induced adaptive responses. Besides FOXM1, other factors such as epidermal growth factor receptor (EGFR) and c-MET heterodimer,<sup>45</sup> 53BP1,<sup>46,47</sup> and Schlafen 11<sup>48,49</sup> also regulate resistance to PARPis. Therefore, it would be interesting for future studies to examine whether DUXAP8 acts through other mechanisms to regulate HCC resistance to PARPis.

In summary, here, we report the biological and clinical significance of the DUXAP8/FOXM1 axis in HCC and reveal two novel regulatory mechanisms between these two molecules. This study provides substantial evidence that targeting DUXAP8 or upregulating miR-485-5p suppresses HCC progression and enhances the sensitivity to PARPis. Considering the extended regulatory networks known to involve DUXAP8, miR-485-5p, or FOXM1 in cancer development, it is important to assess the importance of this axis in other types of cancer.

## MATERIALS AND METHODS

### Human Samples and Database Analysis

A cohort of 52 pairs of tumor tissues and matching para-tumor normal tissues were obtained during surgery between January 2018 and October 2019 from HCC patients admitted into the Department of General Surgery, Xiangya Hospital, Central South University (Hunan, P.R. China). The diagnosis was established by pathological examinations. Clinicopathological features of all HCC cases were recorded and are summarized in Table 1. Written consents were obtained from all participants, and the study was approved by the Ethics Committee of Xiangya Hospital. TCGA analysis was performed using the GEPIA as described previously.<sup>50</sup>

### Human Cancer Cell Lines and Reagents

The normal human liver epithelial cell line THLE-3; HCC cell lines HCCC9810, BEL-7402, HUH-7, SMMC-7721, and HepG2; and the

multiple drug-resistant HepG2/adriamycin (HepG2/ADR)<sup>51</sup> were purchased from the Cell Bank of the Chinese Academy of Sciences (Shanghai, P.R. China). THLE-3 cells were cultured in BEGM medium supplemented with the BEGM Bullet Kit (Lonza, Walkersville, MD, USA), and all HCC cells were cultured in Dulbecco's modified Eagle's medium (DMEM; Invitrogen, Carlsbad, CA, USA) containing 10% fetal bovine serum (Invitrogen) and 1% penicillin/streptomycin. All cells were maintained in a sterile humidified atmosphere containing 5% CO<sub>2</sub> at 37°C.

Olaparib (AZD2281) was purchased from MCE (Shanghai, P.R. China), dissolved in DMSO, and reconstituted to 10 mM with H<sub>2</sub>O.

#### Reverse Transcription Followed by Quantitative Real-Time PCR

Quantitative real-time PCR was performed as described previously<sup>52</sup> using the following primers for the corresponding human genes: U6 (internal control for lncRNA or miRNA) forward primer, 5'-CTCGCTTCGGCAGCACA-3', and reverse primer, 5'-AACGCTTCACGAA TTTGCGT-3'; DUXAP8 forward primer, 5'-AGGATGGAGTCTCGCTGTATTGC-3', and reverse primer, 5'-GGAGTTTGTCTTCTTTT-3'; miR-485-5p forward primer, 5'-AGAGGCTGGCCGTGAT-3', and reverse primer 5'-GAACATGTCTGCGTATCTC-3'; FOXM1 forward primer, 5'-TCTGCCAATGGCAAGGTCTCCT-3', and reverse primer, 5'-CTGGATTCCGGTCGTTTCTGCTG-3'; CDK6 forward primer, 5'-GGATAAAGTTCCAGAGCCTGGAG-3', and reverse primer, 5'-GCGATGCACTACTCGGTGTGAA-3'; CCNB1 forward primer, 5'-GACCTGTGTCAGGCTTCTCTG-3', and reverse primer, 5'-GGTATTTTGGTCTGACTGCTTGC-3'; BRCA1 forward primer, 5'-CTGAAGACTGCTCAGGGCTATC-3', and reverse primer, 5'-AGGGTAGCTGTTAGAAGGCTGG-3'; RAD51 forward primer, 5'-TCTCTGGCAGTGATGTCCTGGA-3', and reverse primer, 5'-TAAAGGGCGGTGGCACTGTCTA-3'; GAPDH (internal control for mRNA) forward primer, 5'-GTCTCCTCTGACTTCAACAGCG-3', and reverse primer, 5'-ACCACCCTGTTGCTGTAGCCAA-3'. The relative expression of a target gene was calculated using the 2<sup>-ΔΔCt</sup> method.<sup>53</sup>

#### Construction of Lentivirus and Generation of Stable Cells

shDUXAP8, shNC, human miR-485-5p mimic, and mimic NC were purchased from GenePharma (Shanghai, P.R. China). shDUXAP8 or shNC sequences were cloned into lentiviral vector pLKO.1-puro (Sigma, St. Louis, MO, USA). To produce lentivirus, lentiviral vector was co-transfected into HEK293T cells with packaging vectors using the Lentiviral Packaging Kit (OriGene, Rockville, MD, USA) according to the manufacturer's protocol. After 48 h, lentivirus-containing supernatant was harvested from the culture, centrifuged at 500 × g for 5 min to remove cell debris, and applied to target cells in the presence of polybrene (8 μg/mL; Sigma) overnight. Then, target cells were cultured in fresh complete growth medium for 48 h and selected in medium containing puromycin (5 μg/mL) for a further 10 days.

To overexpress FOXM1 or FUS, the human FOXM1 or FUS cDNA sequence was cloned into pcDNA3.1 vector (Thermo Fisher Scientific, Waltham, MA, USA). The empty vector was used as the NC. The

transfection of pcDNA3.1 vector or miRNA mimics was performed using Lipofectamine 3000 (Invitrogen) according to the manufacturer's instructions.

#### Cell Viability Assay

Cell viability was measured using the MTT assay. Briefly, cells were seeded in 96-well plates at a density of 2 × 10<sup>4</sup> cells per milliliter and incubated for 6, 12, 24, 48, or 72 h. MTT solution (5 mg/mL in PBS, 20 μL per well; Sigma) was added to each well and allowed to incubate with cells at 37°C for 3 h. The medium was then replaced with 100 μL dimethyl sulfoxide (DMSO; Sigma) and incubated with cells for a further 2 h in the dark at room temperature. Finally, the optical density of formazan crystals dissolved by DMSO (proportional to the number of live cells) was measured with the Bio-Rad 550 Microplate Reader at 490 nm.

#### Colony-Forming Assay

The long-term proliferation of cells was measured using a colony-forming assay. Briefly, target cells were seeded into a 24-well plate at 200 cells per well. After incubating the cells at 37°C for 10 days, cells were fixed with 100% methanol (Sigma) at room temperature for 10 min and then stained with 0.5% crystal violet (Sigma) at room temperature for 5 min. The number of cell colonies was counted under a light microscope.

#### Transwell Migration/Invasion Assay

A Transwell assay was performed as previously described.<sup>54</sup> Briefly, the single-cell suspension of target cells was seeded into the top well (1 × 10<sup>5</sup> cells per well) of Transwell inserts (8.0 μm; Corning, Lowell, MA, USA; either uncoated for migration assay or coated with Matrigel from BD Biosciences, San Jose, CA, USA, for invasion assay) and cultured in serum-free DMEM medium at 37°C. In the lower chamber, 500 μL DMEM containing 10% fetal bovine serum was added. After 24 h, the non-migrating/invading cells were removed from the top of the membrane, and those that migrated or invaded through the membrane were fixed in 95% methanol, stained with 1% crystal violet, and counted under an inverted microscope (100×).

#### Western Immunoblots

Total proteins were extracted from cultured cells using RIPA buffer (Thermo Fisher Scientific) and separated on 10% SDS-PAGE gel. Following the transfer of separated proteins onto a polyvinylidene difluoride membrane, the membrane was blocked with 5% nonfat milk in TBST (10 mM Tris [pH 8.0], 150 mM NaCl, 0.5% Tween 20) at room temperature for 1 h, washed three times in TBST, and incubated with one of the following primary antibodies (all from Cell Signaling Technology, Danvers, MA, USA, unless otherwise indicated): E-cadherin (1:1,000; #14472), N-cadherin (1:1,000; #13116), Vimentin (1:1,000; #5741), Slug (1:1,000; #9585), FOXM1 (1:1,000; #5436), BRCA1 (1:1,000; #14823), RAD51 (1:1,000; #8875), or β-actin (1:5,000; #3700; internal control) at 4°C overnight. After three washes with TBST, the membrane was incubated with horseradish-peroxidase-conjugated secondary antibodies at room temperature for 2 h.

The signal was developed using an enhanced chemiluminescence system (Beyotime, Jiangsu, P.R. China) according to the manufacturer's instructions.

#### **In Vivo Xenograft Growth and Experimental Metastasis Assays**

Female athymic BALB/c nude mice (4–6 weeks old) were purchased from Hunan SJA Laboratory Animals (Hunan, P.R. China) and maintained under pathogen-free conditions. To monitor *in vivo* xenograft growth, BEL-7402 cells stably transfected with shDUXAP8 versus shNC were subcutaneously injected into the dorsal flank region of each mouse ( $1 \times 10^6$  cells per injection,  $n = 4$  per group). Tumor growth was measured every 3 days using a vernier caliper, and the tumor volume (V) was calculated as:  $V = 1/2 \times \text{length} \times \text{width}$ .<sup>2</sup> On day 21 after the inoculation of HCC cells, all mice were euthanized, and xenografts were examined. To examine the experimental metastasis, BEL-7402 cells stably transfected with shDUXAP8 versus shNC were intravenously injected into each mouse through the tail vein ( $1 \times 10^6$  cells per injection;  $n = 5$  per group). After 30 days, mice were sacrificed, and the lungs were excised, imaged, and processed for histological analysis. All animal protocols were reviewed and approved by the Institutional Animal Care and Use Committee of Xiangya Hospital.

#### **Histological Analysis**

Upon fixation in 10% formalin and embedded in paraffin, mouse tissues were processed into 4- $\mu\text{m}$  sections. Staining with H&E was performed using an H&E staining kit (Vector Laboratories, Burlingame, CA, USA) according to the manufacturer's instructions. For immunohistochemical (IHC) staining for Ki67 and FOXM1, tissue sections underwent antigen retrieval in boiling 10 mM citrate buffer (pH 6.0) for 10 min and blocked for endogenous peroxidase activity using 0.3%  $\text{H}_2\text{O}_2$  for 10 min followed by non-specific binding using 5% normal goat serum for 1 h at room temperature. The tissue sections were incubated with anti-Ki67 (1:400, #9449) or anti-FOXM1 (1:600, #20459) antibody (both from Cell Signaling Technology) at 4°C overnight, followed by biotinylated secondary antibody at room temperature for 30 min, and then with Vectastain ABC-HRP solution (Vector Labs) at room temperature for 30 min, with TBST washes in between. The signal was developed using diaminobenzidine (DAB) substrate (Vector Labs), and the slides were counterstained with hematoxylin.

#### **Luciferase Reporter Assay**

We used the starBase platform (<http://starbase.sysu.edu.cn/>) and identified miR-485-5p as a miRNA that could interact with both DUXAP8 and FOXM1. Mutations were introduced into the potential binding sequences of DUXAP8 and FOXM1, respectively. The WT and MUT binding sequences were cloned into pRL-CMV luciferase reporter plasmid. BEL-7402 cells were co-transfected with the luciferase reporter plasmid and miR-485-5p mimic or control mimic (mimic NC) using Lipofectamine 3000. At 48 h following the transfection, luciferase activity was detected using the Dual Luciferase Reporter Assay System (Promega, Madison, WI, USA) according to the manufacturer's instructions.<sup>55</sup>

#### **RIP**

To examine the potential binding between FUS and DUXAP8 or FOXM1 mRNA, a RIP assay was performed using the Magna RIP RNA-Binding Protein Immunoprecipitation Kit (17-700, Millipore) following the manufacturer's instructions. Briefly, whole-cell lysate was incubated with anti-FUS antibody (ab70381, Abcam, Cambridge, MA, USA) conjugated to protein A/G Sepharose beads at 4°C for 6 h. Immunoprecipitated RNA was then detected by qPCR and presented as a fold change relative to the amount of RNA co-precipitated with control IgG.

#### **RNA Pull-Down Assays**

WT and MUT DUXAP8 RNAs were *in vitro* transcribed using T7 RNA polymerase (Roche, Basel Switzerland), treated with RNase-free DNase I (Roche, Indianapolis, IN, USA), and purified with the RNeasy Mini Kit (QIAGEN, Germantown, MD, USA). Transcribed RNAs were biotin-labeled with the Biotin RNA Labeling Mix (Roche Diagnostics, Indianapolis, IN, USA). Biotinylated RNAs were then incubated with BEL-7402 cell lysates. Streptavidin-conjugated magnetic beads were added, and the eluted proteins were detected by western blot analysis.

#### **Assay for mRNA Decay**

The measurement of mRNA decay was performed as described previously.<sup>56,57</sup> Briefly, shDUXAP8- or shNC-expressing BEL-7402 cells were transfected with either FUS-expressing vector or empty vector. After 48 h, cells were treated with actinomycin D to inhibit transcription (0 h). The FOXM1 mRNA level was then measured using quantitative real-time PCR at indicated time points and presented as a relative ratio to that at the 0-h time point.

#### **Statistical Analysis**

All data were analyzed by GraphPad Prism 6.0 and presented as means  $\pm$  SD from at least three independent experiments (for *in vitro* assays) or from multiple mice within each group (for *in vivo* assays). Differences between experimental groups were assessed by the Student's t test or one-way ANOVA. A p value of less than 0.05 was considered statistically significant.

#### **ACKNOWLEDGMENTS**

None.

#### **AUTHOR CONTRIBUTIONS**

Guarantor of integrity of the entire study: Q.Z.; study concepts: Q.Z., Y.H., and H.-Y.Z.; study design: Q.Z., Y.H., and H.-Y.Z.; definition of intellectual content: Y.H. and Q.Z.; literature research: Y.H., L.X., and W.J.; clinical studies: Q.Z., Y.H., and L.X.; experimental studies: Y.H., Q.Z., L.X., and W.J.; data acquisition: X.Z. and Q.Z.; data analysis: X.Z. and Q.Z.; statistical analysis: X.Z. and Y.H.; manuscript preparation: Y.H. and Q.Z.; manuscript editing: Y.H. and Q.Z.; manuscript review: Y.H., Q.Z., and H.-Y.Z..

#### **DECLARATION OF INTEREST**

The authors declare no competing interests.

## REFERENCES

- Bray, F., Ferlay, J., Soerjomataram, I., Siegel, R.L., Torre, L.A., and Jemal, A. (2018). Global cancer statistics 2018: GLOBOCAN estimates of incidence and mortality worldwide for 36 cancers in 185 countries. *CA Cancer J. Clin.* 68, 394–424.
- Zhu, R.X., Seto, W.K., Lai, C.L., and Yuen, M.F. (2016). Epidemiology of Hepatocellular Carcinoma in the Asia-Pacific Region. *Gut Liver* 10, 332–339.
- Selçuk, H. (2017). Prognostic Factors and Staging Systems in Hepatocellular Carcinoma. *Exp. Clin. Transplant.* 15 (Suppl 2), 45–49.
- Rouleau, M., Patel, A., Hendzel, M.J., Kaufmann, S.H., and Poirier, G.G. (2010). PARP inhibition: PARP1 and beyond. *Nat. Rev. Cancer* 10, 293–301.
- He, C., Kawaguchi, K., and Toi, M. (2020). DNA damage repair functions and targeted treatment in breast cancer. *Breast Cancer* 27, 355–362.
- Sunada, S., Nakanishi, A., and Miki, Y. (2018). Crosstalk of DNA double-strand break repair pathways in poly(ADP-ribose) polymerase inhibitor treatment of breast cancer susceptibility gene 1/2-mutated cancer. *Cancer Sci.* 109, 893–899.
- Kubalanza, K., and Konecny, G.E. (2020). Mechanisms of PARP inhibitor resistance in ovarian cancer. *Curr. Opin. Obstet. Gynecol.* 32, 36–41.
- Wakefield, M.J., Nestic, K., Kondrashova, O., and Scott, C.L. (2019). Diverse mechanisms of PARP inhibitor resistance in ovarian cancer. *Biochim. Biophys. Acta Rev. Cancer* 1872, 188307.
- Fang, P., Madden, J.A., Neums, L., Moulder, R.K., Forrest, M.L., and Chien, J. (2018). Olaparib-induced Adaptive Response Is Disrupted by FOXM1 Targeting that Enhances Sensitivity to PARP Inhibition. *Mol. Cancer Res.* 16, 961–973.
- Gabrielson, A., Tesfaye, A.A., Marshall, J.L., Pishvaian, M.J., Smaglo, B., Jha, R., Dorsch-Vogel, K., Wang, H., and He, A.R. (2015). Phase II study of temozolomide and veliparib combination therapy for sorafenib-refractory advanced hepatocellular carcinoma. *Cancer Chemother. Pharmacol.* 76, 1073–1079.
- Jiang, M.C., Ni, J.J., Cui, W.Y., Wang, B.Y., and Zhuo, W. (2019). Emerging roles of lncRNA in cancer and therapeutic opportunities. *Am. J. Cancer Res.* 9, 1354–1366.
- Gong, W.J., Yin, J.Y., Li, X.P., Fang, C., Xiao, D., Zhang, W., Zhou, H.H., Li, X., and Liu, Z.Q. (2016). Association of well-characterized lung cancer lncRNA polymorphisms with lung cancer susceptibility and platinum-based chemotherapy response. *Tumour Biol.* 37, 8349–8358.
- Peng, L., Yuan, X., Jiang, B., Tang, Z., and Li, G.C. (2016). lncRNAs: key players and novel insights into cervical cancer. *Tumour Biol.* 37, 2779–2788.
- Yue, C., Liang, C., Li, P., Yan, L., Zhang, D., Xu, Y., Wei, Z., and Wu, J. (2019). DUXAP8 a Pan-Cancer Prognostic Marker Involved in the Molecular Regulatory Mechanism in Hepatocellular Carcinoma: A Comprehensive Study Based on Data Mining, Bioinformatics, and in vitro Validation. *OncoTargets Ther.* 12, 11637–11650.
- Jiang, H., Shi, X., Ye, G., Xu, Y., Xu, J., Lu, J., and Lu, W. (2019). Up-regulated long non-coding RNA DUXAP8 promotes cell growth through repressing Krüppel-like factor 2 expression in human hepatocellular carcinoma. *OncoTargets Ther.* 12, 7429–7436.
- Guillot, C., Hall, J., Herceg, Z., Merle, P., and Chemin, I. (2014). Update on hepatocellular carcinoma breakthroughs: poly(ADP-ribose) polymerase inhibitors as a promising therapeutic strategy. *Clin. Res. Hepatol. Gastroenterol.* 38, 137–142.
- Li, W., Yang, W., and Wang, X.J. (2013). Pseudogenes: pseudo or real functional elements? *J. Genet. Genomics* 40, 171–177.
- Milligan, M.J., and Lipovich, L. (2015). Pseudogene-derived lncRNAs: emerging regulators of gene expression. *Front. Genet.* 5, 476.
- Groen, J.N., Capraro, D., and Morris, K.V. (2014). The emerging role of pseudogene expressed non-coding RNAs in cellular functions. *Int. J. Biochem. Cell Biol.* 54, 350–355.
- Lian, Y., Yang, J., Lian, Y., Xiao, C., Hu, X., and Xu, H. (2018). DUXAP8, a pseudogene derived lncRNA, promotes growth of pancreatic carcinoma cells by epigenetically silencing CDKN1A and KLF2. *Cancer Commun. (Lond.)* 38, 64.
- Sun, M., Nie, F.Q., Zang, C., Wang, Y., Hou, J., Wei, C., Li, W., He, X., and Lu, K.H. (2017). The Pseudogene DUXAP8 Promotes Non-small-cell Lung Cancer Cell Proliferation and Invasion by Epigenetically Silencing EGFR and RHOB. *Mol. Ther.* 25, 739–751.
- Ma, H.W., Xie, M., Sun, M., Chen, T.Y., Jin, R.R., Ma, T.S., Chen, Q.N., Zhang, E.B., He, X.Z., De, W., and Zhang, Z.H. (2016). The pseudogene derived long noncoding RNA DUXAP8 promotes gastric cancer cell proliferation and migration via epigenetically silencing PLEKHO1 expression. *Oncotarget* 8, 52211–52224.
- Gong, A., Huang, Z., Ge, H., Cai, Y., and Yang, C. (2019). The carcinogenic complex lncRNA DUXAP8/EZH2/LSD1 accelerates the proliferation, migration and invasion of colorectal cancer. *J. BUON* 24, 1830–1836.
- Du, C., Wang, H.X., Chen, P., and Chen, C.H. (2019). STAT3-induced upregulation of lncRNA DUXAP8 functions as ceRNA for miR-577 to promote the migration and invasion in colorectal cancer through the regulation of RAB14. *Eur. Rev. Med. Pharmacol. Sci.* 23, 6105–6118.
- Huang, T., Wang, X., Yang, X., Ji, J., Wang, Q., Yue, X., and Dong, Z. (2018). Long Non-Coding RNA DUXAP8 Enhances Renal Cell Carcinoma Progression via Downregulating miR-126. *Med. Sci. Monit.* 24, 7340–7347.
- Duan, J., Zhang, H., Li, S., Wang, X., Yang, H., Jiao, S., and Ba, Y. (2017). The role of miR-485-5p/NUDT1 axis in gastric cancer. *Cancer Cell Int.* 17, 92.
- Kang, M., Ren, M.P., Zhao, L., Li, C.P., and Deng, M.M. (2015). miR-485-5p acts as a negative regulator in gastric cancer progression by targeting flotillin-1. *Am. J. Transl. Res.* 7, 2212–2222.
- Gao, F., Wu, H., Wang, R., Guo, Y., Zhang, Z., Wang, T., Zhang, G., Liu, C., and Liu, J. (2019). MicroRNA-485-5p suppresses the proliferation, migration and invasion of small cell lung cancer cells by targeting flotillin-2. *Bioengineered* 10, 1–12.
- Lou, C., Xiao, M., Cheng, S., Lu, X., Jia, S., Ren, Y., and Li, Z. (2016). MiR-485-3p and miR-485-5p suppress breast cancer cell metastasis by inhibiting PGC-1 $\alpha$  expression. *Cell Death Dis.* 7, e2159.
- Wang, M., Cai, W.R., Meng, R., Chi, J.R., Li, Y.R., Chen, A.X., Yu, Y., and Cao, X.C. (2018). miR-485-5p suppresses breast cancer progression and chemosensitivity by targeting survivin. *Biochem. Biophys. Res. Commun.* 501, 48–54.
- Li, G., and Kong, Q. (2019). lncRNA LINC00460 promotes the papillary thyroid cancer progression by regulating the LINC00460/miR-485-5p/Raf1 axis. *Biol. Res.* 52, 61.
- Zhang, Y., Hu, J., Zhou, W., and Gao, H. (2018). lncRNA FOXD2-AS1 accelerates the papillary thyroid cancer progression through regulating the miR-485-5p/CLK7 axis. *J. Cell. Biochem. Published November 19, 2018.* <https://doi.org/10.1002/jcb.28072>.
- Peng, Y., Leng, W., Duan, S., and Hong, M. (2019). Long noncoding RNA BLACAT1 is overexpressed in hepatocellular carcinoma and its downregulation suppressed cancer cell development through endogenously competing against hsa-miR-485-5p. *Biomed. Pharmacother.* 116, 109027.
- Sun, X., Liu, Y., Li, M., Wang, M., and Wang, Y. (2015). Involvement of miR-485-5p in hepatocellular carcinoma progression targeting EMMPRIN. *Biomed. Pharmacother.* 72, 58–65.
- Tu, J., Zhao, Z., Xu, M., Chen, M., Weng, Q., and Ji, J. (2019). LINC00460 promotes hepatocellular carcinoma development through sponging miR-485-5p to up-regulate PAK1. *Biomed. Pharmacother.* 118, 109213.
- Wang, Y., Sun, L., Wang, L., Liu, Z., Li, Q., Yao, B., Wang, C., Chen, T., Tu, K., and Liu, Q. (2018). Long non-coding RNA DSCR8 acts as a molecular sponge for miR-485-5p to activate Wnt/ $\beta$ -catenin signal pathway in hepatocellular carcinoma. *Cell Death Dis.* 9, 851.
- Colombrita, C., Onesto, E., Megiorni, F., Pizzuti, A., Baralle, F.E., Buratti, E., Silani, V., and Ratti, A. (2012). TDP-43 and FUS RNA-binding proteins bind distinct sets of cytoplasmic messenger RNAs and differently regulate their post-transcriptional fate in motoneuron-like cells. *J. Biol. Chem.* 287, 15635–15647.
- Zheng, L.L., Zhou, K.R., Liu, S., Zhang, D.Y., Wang, Z.L., Chen, Z.R., Yang, J.H., and Qu, L.H. (2018). dreamBase: DNA modification, RNA regulation and protein binding of expressed pseudogenes in human health and disease. *Nucleic Acids Res.* 46 (D1), D85–D91.
- Bao, L., Yuan, L., Li, P., Bu, Q., Guo, A., Zhang, H., Cui, N., and Liu, B. (2018). A FUS-LATS1/2 Axis Inhibits Hepatocellular Carcinoma Progression via Activating Hippo Pathway. *Cell. Physiol. Biochem.* 50, 437–451.
- Ge, Z., Cheng, Z., Yang, X., Huo, X., Wang, N., Wang, H., Wang, C., Gu, D., Zhao, F., Yao, M., et al. (2017). Long noncoding RNA SchLAH suppresses metastasis of

- hepatocellular carcinoma through interacting with fused in sarcoma. *Cancer Sci.* *108*, 653–662.
41. Guo, T., Wang, H., Liu, P., Xiao, Y., Wu, P., Wang, Y., Chen, B., Zhao, Q., Liu, Z., and Liu, Q. (2018). SNHG6 Acts as a Genome-Wide Hypomethylation Trigger via Coupling of miR-1297-Mediated S-Adenosylmethionine-Dependent Positive Feedback Loops. *Cancer Res.* *78*, 3849–3864.
  42. Li, L., Zhao, H., Chen, B., Huang, K., Hao, Z., Fan, Z., Sun, G., Wu, J., Li, N., Ye, Q., and Yue, J. (2019). Noninvasive Identification of Immune-Related Biomarkers in Hepatocellular Carcinoma. *J. Oncol.* *2019*, 2531932.
  43. Wierstra, I. (2013). FOXM1 (Forkhead box M1) in tumorigenesis: overexpression in human cancer, implication in tumorigenesis, oncogenic functions, tumor-suppressive properties, and target of anticancer therapy. *Adv. Cancer Res.* *119*, 191–419.
  44. Liao, G.B., Li, X.Z., Zeng, S., Liu, C., Yang, S.M., Yang, L., Hu, C.J., and Bai, J.Y. (2018). Regulation of the master regulator FOXM1 in cancer. *Cell Commun. Signal.* *16*, 57.
  45. Dong, Q., Du, Y., Li, H., Liu, C., Wei, Y., Chen, M.K., Zhao, X., Chu, Y.Y., Qiu, Y., Qin, L., et al. (2019). EGFR and c-MET Cooperate to Enhance Resistance to PARP Inhibitors in Hepatocellular Carcinoma. *Cancer Res.* *79*, 819–829.
  46. Becker, J.R., Cuella-Martin, R., Barazas, M., Liu, R., Oliveira, C., Oliver, A.W., Bilham, K., Holt, A.B., Blackford, A.N., Heierhorst, J., et al. (2018). The ASCIZ-DYNLL1 axis promotes 53BP1-dependent non-homologous end joining and PARP inhibitor sensitivity. *Nat. Commun.* *9*, 5406.
  47. Gupta, R., Somyajit, K., Narita, T., Maskey, E., Stanlie, A., Kremer, M., Typas, D., Lammers, M., Mailand, N., Nussenzweig, A., et al. (2018). DNA Repair Network Analysis Reveals Shieldin as a Key Regulator of NHEJ and PARP Inhibitor Sensitivity. *Cell* *173* (4), 972–988.e23.
  48. Stewart, C.A., Tong, P., Cardnell, R.J., Sen, T., Li, L., Gay, C.M., Masrorpour, F., Fan, Y., Bara, R.O., Feng, Y., et al. (2017). Dynamic variations in epithelial-to-mesenchymal transition (EMT), ATM, and SLFN11 govern response to PARP inhibitors and cisplatin in small cell lung cancer. *Oncotarget* *8*, 28575–28587.
  49. Murai, J., Feng, Y., Yu, G.K., Ru, Y., Tang, S.W., Shen, Y., and Pommier, Y. (2016). Resistance to PARP inhibitors by SLFN11 inactivation can be overcome by ATR inhibition. *Oncotarget* *7*, 76534–76550.
  50. Tang, Z., Li, C., Kang, B., Gao, G., Li, C., and Zhang, Z. (2017). GEPIA: a web server for cancer and normal gene expression profiling and interactive analyses. *Nucleic Acids Res.* *45* (W1), W98–W102.
  51. Sun, L., Chen, W., Qu, L., Wu, J., and Si, J. (2013). Icaritin reverses multidrug resistance of HepG2/ADR human hepatoma cells via downregulation of MDR1 and P-glycoprotein expression. *Mol. Med. Rep.* *8*, 1883–1887.
  52. Zhu, Q., Wang, Z., Hu, Y., Li, J., Li, X., Zhou, L., and Huang, Y. (2012). miR-21 promotes migration and invasion by the miR-21-PDCD4-AP-1 feedback loop in human hepatocellular carcinoma. *Oncol. Rep.* *27*, 1660–1668.
  53. Livak, K.J., and Schmittgen, T.D. (2001). Analysis of relative gene expression data using real-time quantitative PCR and the 2<sup>(-Delta Delta C(T))</sup> Method. *Methods* *25*, 402–408.
  54. Liu, Y., and Liu, B.A. (2011). Enhanced proliferation, invasion, and epithelial-mesenchymal transition of nicotine-promoted gastric cancer by periostin. *World J. Gastroenterol.* *17*, 2674–2680.
  55. Fang, F., Yang, L., Tao, Y., and Qin, W. (2012). FBI-1 promotes cell proliferation and enhances resistance to chemotherapy of hepatocellular carcinoma in vitro and in vivo. *Cancer* *118*, 134–146.
  56. Di, W., Weinan, X., Xin, L., Zhiwei, Y., Xinyue, G., Jinxue, T., and Mingqi, L. (2019). Long noncoding RNA SNHG14 facilitates colorectal cancer metastasis through targeting EZH2-regulated EPHA7. *Cell Death Dis.* *10*, 514.
  57. Zhang, L., Yang, Z., Trotter, J., Barbier, O., and Wang, L. (2017). Long noncoding RNA MEG3 induces cholestatic liver injury by interaction with PTBP1 to facilitate shp mRNA decay. *Hepatology* *65*, 604–615.